

Article

Microstructural Evolution in AlMgSi Alloys during Solidification under Electromagnetic Stirring

Piotr Mikolajczak

Institute of Materials Technology, Poznan University of Technology, Piotrowo 3, 60-965 Poznan, Poland; Piotr.Mikolajczak@put.poznan.pl; Tel.: +48-61-66-52-804

Academic Editor: Mohsen Asle Zaeem

Received: 19 December 2016; Accepted: 6 March 2017; Published: 10 March 2017

Abstract: Equiaxed solidification of AlMgSi alloys with Fe and Mn was studied by electromagnetic stirring to understand the effect of forced flow. The specimens solidified with a low cooling rate, low temperature gradient, and forced convection. Stirring induced by a coil system around the specimens caused a transformation from equiaxed dendritic to rosette morphology with minor dendrites and, occasionally, spheroids. This evolution was quantitatively observed with specific surface S_v . The precipitation sequence of the phases was calculated using the CALPHAD (Computer Coupling of Phase Diagrams and Thermochemistry) technique. Melt flow decreased secondary dendrite arm spacing λ_2 in the AlSi5Fe1.0 alloy, while λ_2 increased slightly in Mg-containing alloys. The length of detrimental β -Al₅FeSi phases decreased only in AlSi5Fe1.0 alloy under stirring, whereas in Mg-containing alloys, changes to the β -Al₅FeSi phase were negligible; however, in all specimens, the number density increased. The modification of Mn-rich phases, spacing of eutectics, and Mg₂Si phases was analyzed. It was found that the occurrence of Mg₂Si phase regions reduced fluid flow in the late stages of solidification and, consequentially, reduced shortening of β -Al₅FeSi, diminished secondary arm-ripening caused by forced convection, and supported diffusive ripening. However, the Mg₂Si phase was found to have not disturbed stirring in the early stage of solidification, and transformation from dendrites to rosettes was unaffected.

Keywords: aluminum alloys; electromagnetic stirring; dendrite arm spacing; rosettes; Mg₂Si phases; solidification

1. Introduction

Aluminum alloys have widespread applications, especially in the aerospace and automotive industries. Aluminum–silicon alloys are particularly widely used (e.g., types A355, A356, A357, AK51, AK7, AG10). Increasing demands on such material properties as tensile strength, corrosion behavior, and ductility have pointed to the need for precise control of microstructure through exact casting practice, composition, and heat treatment.

In the presence of forced convection, non-dendritic structures may form, with the primary α -Al phase shaped as rosettes or spheroids (globular) [1]. Such non-dendritic structures exhibit distinctive rheological properties, making semisolid metal (SSM) and thixoforming [2] unique for near net shape production of engineering parts. In this technique, semisolid slurries with globular solid particles may be obtained by mechanical stirring or magnetohydrodynamic (MHD) stirring. Rotating magnetic fields can modify the microstructure [3]—for example, by changing direction of dendrites [4]—and improve properties of castings.

In this work, the effect of Fe, Mn, and Mg on AlSi alloys was particularly studied. Among many elements used, iron is considered the most deleterious in cast aluminum because the β -Al₅FeSi intermetallic phases that form are particularly detrimental to the ductility of the material [5].

Manganese is the most common alloying addition applied to modify the morphology and type of intermetallic phases in Al alloys. It has been observed previously that Fe and Mn intermetallics, in combination with flow, have different effects on microstructure, and it is possible to transform needle-like Fe phases to blocky ones. Finally, the presence of Mg causes formation of a Mg_2Si phase [6]. This is of interest because recent increases in the application of light Mg alloys and their subsequent recycling may lead to higher amounts of this element in Al alloys.

Here, the influence of stirring during slow cooling of bulk specimens solidifying with equiaxed microstructure has been studied as a function of chemical composition (Mg, Fe, and Mn content) based on Al-5 wt. % Si alloy. The specimens were solidified in controlled thermal conditions, including an induced rotating magnetic field (RMF). Microstructural investigation was carried out via optical metallography with measurements done in ImageJ software. Thermo-Calc [7] was used for calculation of the ternary phase diagram and property diagrams in order to determine the sequence of growth of individual precipitating phases.

2. Materials and Methods

The study investigated five aluminum alloys (AlSi5Fe1.0, AlMg5Si5, AlMg5Si5Fe1.0, AlMg5Si5Mn1.0, and AlMg5Si5-Fe1.0Mn1.0) which were prepared from pure components: Al (99.999% Hydro Aluminum High Purity GmbH, Grevenbroich, DE), Si (99.9999% NewMet House, Essex, UK), Mg (99.99% NewMet House, Essex, UK), Mn (99.98% NewMet House, Essex, UK), and Fe from ferroaluminum (50 wt. % Al-50 wt. % Fe, Goodfellow Cambridge Ltd., Cambridge, UK). The melt was prepared in an electric resistance furnace using a graphite crucible (50 mm inner diameter). From the beginning of the melting process, a continuous flux of argon flushed the crucible and, after melting, the melt was degassed with argon. No modifier was added.

The cylindrical specimens (38 mm diameter and 55 mm height) were melted and solidified in the graphite crucible. Both the crucible and the alloy were heated to 800–810 °C and moved from the furnace into the solidification facility equipped with coils and thermal insulation (Fiberfrax Sibril, Unifrax USA, Tonawanda, NY, USA). The temperature was measured: (1) in the specimen's center; (2) in the specimen, 4 mm from specimen–crucible surface; and (3) in the crucible, 3 mm from specimen–crucible surface. Measured cooling rates achieved: $R_{800\text{-liq}} = 0.626$ (K/s), $R_{\text{liq-sol}} = 0.112$ (K/s), and $R_{\text{sol-470}} = 0.280$ (K/s) for AlSi5Fe1.0 without stirring. Temperature gradient between the specimen center and the location 4 mm from the specimen's surface achieved: $G_{800\text{-liq}} = 0.214$ (K/mm) and $G_{\text{liq-470}} = 0.143$ (K/mm). These measurements proved that common heating and cooling of specimen and crucible assured continuous slow cooling and simultaneous solidification in the whole specimen by using a low temperature gradient and cooling rate, leading to a microstructure with equiaxed dendrites (without RMF stirring).

A rotating magnetic field with a strength of 11 mT (Tesla meter TH26, Aspan, Warsaw, Poland) was generated by electric coils powered by an autotransformer with 45 V and 10 A at a frequency of 50 Hz. The rotational speed was estimated (by camera measurement of the rotating cylinder) to be 2.1 s^{-1} .

The solidified samples (Figure 1) were cut at a height of 10 mm from the bottom for the longitudinal section (Figure 2) and 20 mm from the bottom for the transverse cross-section (Figure 3). The metallographic microsections were prepared using a standard procedure and observed with a light optical microscope (LOM; Nikon, Optiphot-100, Nikon Corp., Tokyo, Japan). In total, 20 sections from 10 experiments were analyzed (5 alloys, each without and with fluid flow). Analysis was performed using Fiji software (ImageJ 1.51a, National Institutes of Health, Bethesda, MD, USA) on the long- and cross-sections in nine specified areas (Figures 2 and 3) using magnifications of $25\times$ and $100\times$.

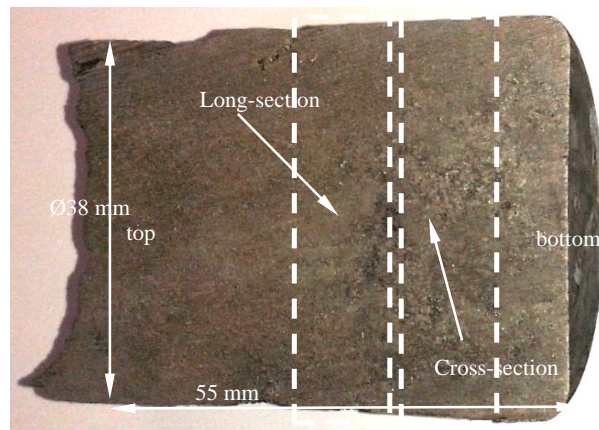


Figure 1. The AlMg5Si5 ingot. The scheme of cutting the long- and cross-section.



Figure 2. The scheme of microstructure parameters' (Table 1) measurement on the long-section—the numbered areas have dimensions $1034 \times 776 \mu\text{m}$ (magnification $100\times$).



Figure 3. The scheme of microstructure parameters (Table 1) measurement on the cross-section—the numbered areas have dimensions $1034 \times 776 \mu\text{m}$ (magnification $100\times$).

For each region, the following parameters were determined: secondary dendrite arm spacing λ_2 , specific surface of the dendrites S_v , average length L_β and number density n_β of $\beta\text{-Al}_5\text{FeSi}$ platelets, and average dimensions L_{Mn} and number density n_{Mn} of $\alpha\text{-Al}_{15}\text{Si}_2\text{Mn}_4$ phases. In addition, the eutectic spacing λ_E for Al–Si eutectics and the spacing $\lambda_{\text{Mg}_2\text{Si}}$ for Mg_2Si phases was measured. The secondary dendrite arm spacing λ_2 was measured by averaging the distance between 20 and 60 adjacent side branches along the primary dendrite stem. Specific surface of the dendrites S_v was calculated from the measured perimeter and the enclosed area of the $\alpha\text{-Al}$ dendrites. In the measurement of about 6500 Fe-rich intermetallics, only needles with a thickness $>3 \mu\text{m}$ and length/thickness ratio >5 were considered. In the measurement of complex-shaped Mn-rich intermetallics, we considered the overall dimensions of each precipitate. The eutectic spacing λ_E was measured by averaging the distance L_E between adjacent eutectic plates; the same was done for Mg_2Si phases.

3. Results

Microstructure on long- and cross-sections of solidified specimens was investigated in 2D micrographs using LOM. The measured parameters are collected in Table 1. The ternary phase diagram, Scheil solidification, and property diagrams were calculated in Thermo-Calc for the studied alloys.

3.1. Microstructure

Figure 4 shows, in AlSi5Fe1.0 alloy micrographs, the typical structures obtained in experiments for solidification without and with stirring. Solidification without flow is characterized by well-formed α -Al dendrites, while for melt stirring, α -Al formed as rosettes and, rarely, as incompletely formed dendrites or as spheroids (globular forms). Figure 5 shows α -Al dendrites (white), (α -Al)-Si eutectic (grey), and β -Al₅FeSi phases (dark grey) in the form of needles spread over the entire sample and only slightly visible, very small β needles. The micrographs (Figures 6 and 7) for AlMg5Si5Fe1.0 additionally show Mg₂Si (very dark) phases arranged between white α -Al dendrites (or rosettes), (α -Al)-Si eutectic (grey), and β -Al₅FeSi needles (dark grey). For AlMg5Si5Mn1.0 alloys, the Fe-rich β needles were replaced by Mn-rich phases with well-developed shapes (Figure 8a) or a more compact form (Figure 8b). For all alloys solidified with electromagnetic stirring, the dendrites changed into rosettes, minor dendrites, or (occasionally) spheroids (Figures 4 and 6).

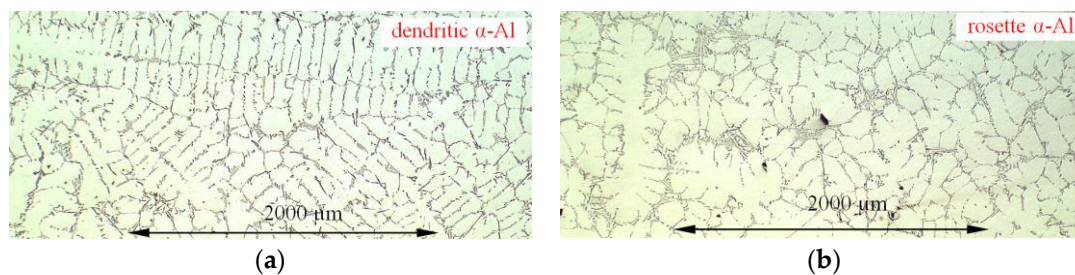


Figure 4. The microstructures of the AlSi5Fe1.0 specimen solidified: (a) without and (b) with electromagnetic stirring. Light optical microscope (LOM), magnification 25 \times .

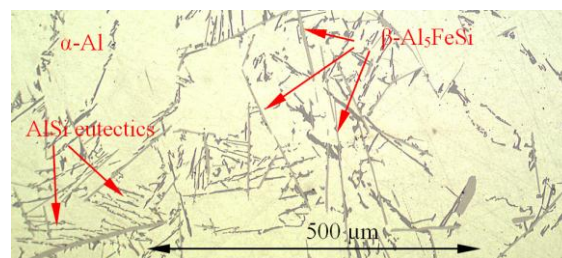


Figure 5. The microstructures of the AlSi5Fe1.0 specimen solidified with electromagnetic stirring. LOM, magnification 100 \times . Clearly visible β -Al₅FeSi phases.

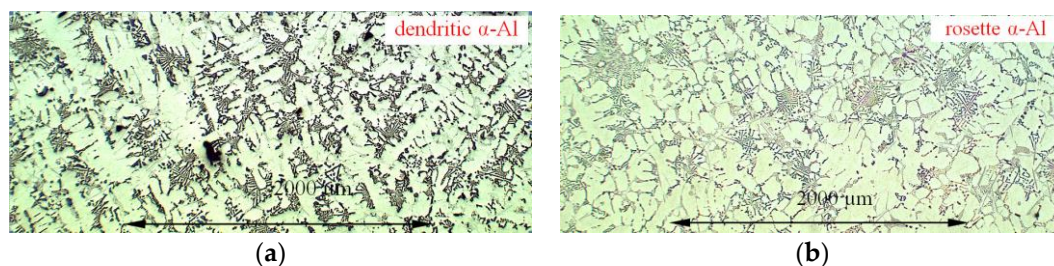


Figure 6. The microstructures of the AlMg5Si5Fe1.0 specimen solidified: (a) without and (b) with electromagnetic stirring. LOM, magnification 25 \times .

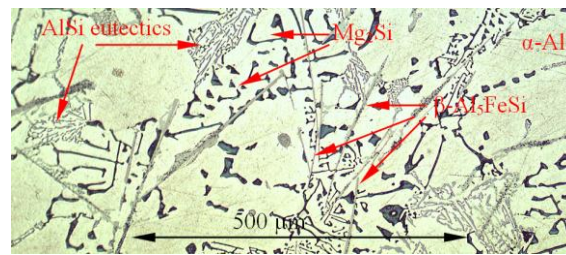


Figure 7. The microstructures of the AlMg5Si5Fe1.0 specimen solidified with electromagnetic stirring. LOM, magnification 100 \times . Highly visible β -Al₅FeSi phases.

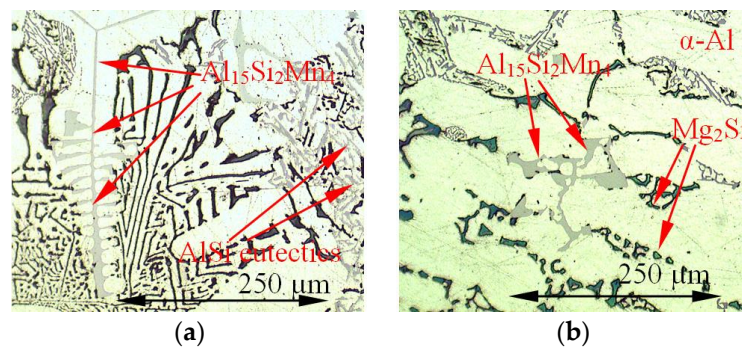


Figure 8. The microstructures of the AlMg5Si5Mn1.0 specimen solidified with electromagnetic stirring rotating magnetic field (RMF). LOM, magnification 100. Highly visible Mn-rich phases: (a) α -Al dendrites grown on Mn-phase; (b) Mn phase grown between dendrites.

3.2. Parameters Characterizing Microstructure

The microstructure evolution caused by electromagnetic stirring is characterized by parameters measured and counted in specified areas (Figures 1–3): nine areas on the cross-section and nine on the long section. The results are almost equal in all 18 figures, and no trend was found across the specimens. Such methodology provides a comprehensive overview of the whole specimen, and credible results are presented in Table 1. For AlSi5Fe1.0, induced fluid flow caused a decrease of about 12% in secondary dendrite arm spacing λ_2 (from 87 to 77 μm), while for the other alloys, λ_2 seems unchanged and reaches values from 60 to 68 μm . Clearly visible in Figures 4 and 6 is the evolution from dendritic to rosette shape, which results in a decrease in the specific surface S_v of α -Al primary phase for all alloys. For the AlSi5Fe1.0 alloy, S_v was found to be 0.023 μm^{-1} for solidification without stirring and 0.019 μm^{-1} with flow, while, for other alloys, stirring caused a decrease from about 0.036 μm^{-1} to about 0.026 μm^{-1} . Stirring caused a decrease in solidification time for all studied alloys.

Fe-rich intermetallics were characterized by average length L_β and by number density n_β . It is clear (Table 1) that fluid flow caused shortening of β phases for AlSi5Fe1.0 alloy, where average length L_β decreased by about 20%, from 71 to 57 μm . The flow effect is much smaller for AlMg5Si5Fe1.0, about 5%, and almost negligible for AlMg5Si5Fe1.0Mn1.0. For all alloys, electromagnetic stirring induced a higher number density of β -Al₅FeSi intermetallics.

Mn-rich intermetallics were characterized by measurement of the average overall dimension L_{Mn} and number density n_{Mn} of mostly complex-shaped precipitates. Fluid flow decreased the average overall dimension L_{Mn} by about 9%, from 299 to 273, and increased number density from 20 to 27 mm^{-2} .

For (α -Al)–Si eutectic, the influence of stirring is unclear; there is no direct modification to the eutectic spacing λ_E . For magnesium-rich Mg₂Si phases, the spacing of $\lambda_{\text{Mg}_2\text{Si}}$ seems to decrease weakly under forced convection. The spacing measured was in the range from 5 to 18 μm .

These measurements were performed on a large number of grains and intermetallics in order to provide highly reliable results. In Table 1, the numbers of grains and dendrite arms inspected are

included in parentheses, while the standard deviations are listed in square brackets. For example, for AlSi5Fe1.0 solidified without stirring we measured 60 grains, 652 dendrite arms, and 1571 β -Al₅FeSi intermetallic phases; standard deviation for λ_2 was 6.7 μm . Stirring caused -12% variation in λ_2 , from 87 to 77 μm , and a decrease in solidification time from 468 to 393 s.

Table 1. Microstructure parameters measured on inspected micrographs.

Aluminium Alloys	RMF (mT) (Solid. Time (s))	Microstructure Parameters							
		Dendrites		Fe-phases (β -Al ₅ FeSi)		Mn-phases		AlSi eutectics	Mg ₂ Si
		λ_{SDAS} (μm)	Sv (μm^{-1})	L_{β} (μm)	n_{β} (mm^{-2})	L_{Mn} (μm)	n_{Mn} (mm^{-2})	λ_{Eut} (μm)	λ_{Mg2Si} (μm)
AlSi5Fe1	0[468]	87 [6.7] (60/652)	0.023 [0.002]	71 [4.1] (1571)	109	-	-	8.5 [0.3]	-
	11[393]	77 [5.7] (68/631) (-12%)	0.019 [0.001] (-17%)	57 [4.1] (2306) (-20%)	160 (47%)	-	-	9.5 [0.3]	-
AlMg5Si5	0[584]	67 [5.1] (134/1135)	0.036 [0.004]	-	-	-	-	9.8 [0.3]	9.7 [0.5] (5-20)
	11[495]	68 [4.0] (109/880)	0.024 [0.002] (-33%)	-	-	-	-	8.8 [0.3]	10.1 [0.5] (4.8-18.6)
AlMg5Si5Fe1	0[537]	60 [4.5] (153/1399)	0.034 [0.003]	79 [4.9] (1043)	72	-	-	11.7 [0.6] [0.6]	11.7 [0.6] (5.3-19.3)
	11[477]	62 [4.0] (150/864)	0.026 [0.002] (-24%)	75 [5.4] (1178) (-5%)	82 (14%)	-	-	6.8 [0.2]	12.7 [0.4] (6.3-18.2)
AlMg5Si5Mn1	0[686]	65 [5.0] (136/1054)	0.036 [0.003]	-	-	299 [13.3]	20	7.5 [0.3]	11.6 [0.7] (5.6-19.0)
	11[638]	65 [4.9] (117/599)	0.028 [0.002] (-24%)	-	-	273 [15.1] (-9%)	27	8.7 [0.2]	12.0 [0.7] (4.3-20.6)
AlMg5Si5Fe1Mn1	0[723]	62 [4.5] (109/678)	0.035 [0.002]	44 [2.2] (128)	9	-	-	8.1 [0.3]	11.3 [0.7] (5.1-18.4)
	11[627]	62 [5.2] (116/382)	0.028 [0.002] (-20%)	43 [2.4] (229) (-2%)	16 (77%)	-	-	9.1 [0.2]	12.1 [0.7] (5.8-19.1)

(1) Curly brackets { ... } present solidification time [s]; (2) brackets [...] present standard deviation; (3) parentheses (... / ...) present numbers of grains inspected and dendrite arms counted; (4) parentheses (... %) present percent variation of the parameters under electromagnetic stirring; (5) parentheses (... - ...) present the range of measured eutectic spacings.

3.3. Precipitation Sequence

On the basis of the ternary Al-Fe-Si phase diagram [7,8] and property diagram (Figure 9), one can state that for the AlSi5Fe1.0 alloy: first, α -Al will form at 627.4 °C ($L \rightarrow \alpha\text{-Al} + L$); then, the liquid enriches in Si and Fe to a concentration of 7.77 %Si and 1.63 %Fe until it reaches the eutectic reaction at 608.4 °C. Next, solidification follows the eutectic groove $L \rightarrow \alpha\text{-Al} + \beta\text{-Al}_5\text{FeSi} + L$ starting from 608.4 °C and ending at 575 °C with composition 12.6 %Si and 0.9 %Fe, where the final eutectic reaction $L \rightarrow \alpha\text{-Al} + \beta\text{-Al}_9\text{Fe}_2\text{Si}_2 + \text{Si}$ occurs. At this point (temperature 575 °C), β -Al₅FeSi mass fraction reaches $f_{\beta} = 3.7\%$, α -Al mass fraction reaches $f_{\alpha} = 93.31\%$, and eutectics mass fraction reaches $f_{Eut} = 2.98\%$. The phase fractions continue to evolve in the solid until, finally, at the temperature 20 °C: $f_{\beta} = 3.7\%$, $f_{\alpha} = 91.63\%$, and $f_{Eut} = 4.67\%$.

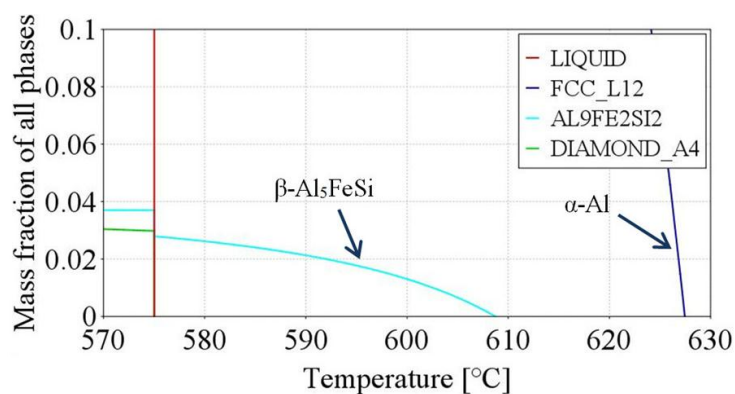


Figure 9. Property diagram for AlSi5Fe1.0 alloy.

Analyzing the solidification path on the ternary Al–Mg–Si phase diagram (Figure 10) and property diagram (Figure 11), one can state that for the AlMg5Si5 alloy: first, α -Al forms at 608.0 °C ($L \rightarrow \alpha\text{-Al} + L$); then, the sample enriches in Si to a concentration of 7.46 %Si and 6.99 %Mg, where it reaches the eutectic reaction at 581.7 °C and α -Al mass fraction reaches $f_{\alpha} = 37.3\%$. Next, solidification follows the eutectic groove $L \rightarrow \alpha\text{-Al} + \text{Mg}_2\text{Si} + L$ starting from 581.7 °C and ending at 558.6 °C with composition 12.5 %Si and 4.5 %Mg, where the final eutectic reaction $L \rightarrow \alpha\text{-Al} + \text{Mg}_2\text{Si} + \text{Si}$ occurs.

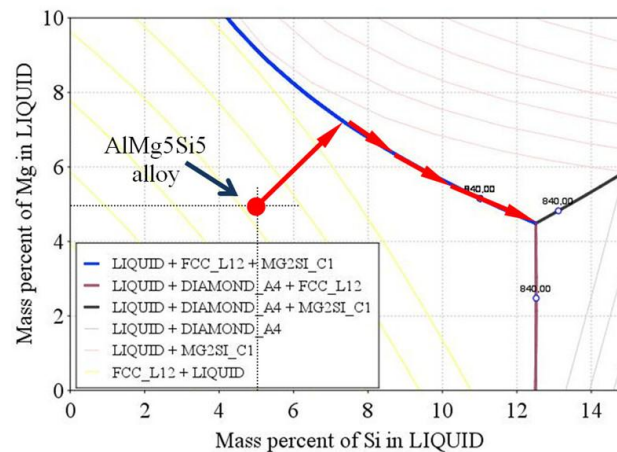


Figure 10. Ternary phase diagram—Al–Si–Mg system. Liquidus projection with red arrows marking the solidification path (Scheil–Gulliver solidification) for AlMg5Si5 alloy.

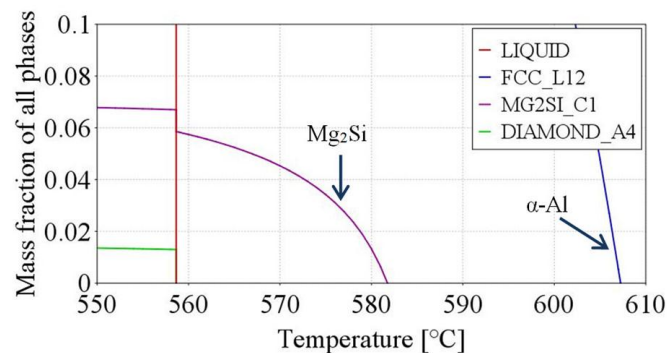


Figure 11. Property diagram for AlMg5Si5 alloy.

For AlMg5Si5Fe1.0 alloy (Figure 12): first, α -Al starts to precipitate at 603.8 °C ($L \rightarrow \alpha\text{-Al} + L$) and continues until 592.5 °C where the α -Al mass fraction reaches $f_{\alpha} = 19.16\%$. At 592.5 °C, $\beta\text{-Al}_8\text{Fe}_2\text{Si}_2$ starts to form according to the reaction $L \rightarrow \alpha\text{-Al} + \beta\text{-Al}_8\text{Fe}_2\text{Si}_2$ and continues until 584.4 °C, where mass fraction reaches $f_{\alpha} = 30.63\%$, $f_{\beta\text{-Al}_8\text{Fe}_2\text{Si}_2} = 0.73\%$. Solidification continues with reaction $L \rightarrow \alpha\text{-Al} + \beta\text{-Al}_9\text{Fe}_2\text{Si}_2$ until 580.9 °C, where mass fraction reaches $f_{\alpha} = 34.75\%$ and $f_{\beta\text{-Al}_9\text{Fe}_2\text{Si}_2} = 1.36\%$. At 580.9 °C, the magnesium phase Mg_2Si starts to form according to $L \rightarrow \alpha\text{-Al} + \beta\text{-Al}_9\text{Fe}_2\text{Si}_2 + \text{Mg}_2\text{Si}$, continuing until 568.9 °C where mass fraction reaches $f_{\alpha} = 73.16\%$, $f_{\beta\text{-Al}_9\text{Fe}_2\text{Si}_2} = 3.19\%$, and $f_{\text{Mg}_2\text{Si}} = 5.10\%$. Finally, the reaction $L \rightarrow \alpha\text{-Al} + \text{Mg}_2\text{Si} + \text{Al}_{18}\text{Fe}_2\text{Mg}_7\text{Si}_{10} + \text{Si}$ commences at 568.9 °C and finishes solidification at 565.5 °C.

The AlMg5Si5Mn1.0 alloy starts to solidify (Figure 13) with the $\text{Al}_{15}\text{Si}_2\text{Mn}_4$ phase at 651.6 °C according to $L \rightarrow \text{Al}_{15}\text{Si}_2\text{Mn}_4 + L$, continuing until 606.0 °C where mass fraction reaches $f_{\text{Al}_{15}\text{Si}_2\text{Mn}_4} = 1.83\%$. The second phase, α -Al, starts to form at 606.0 °C according to $L \rightarrow \text{Al}_{15}\text{Si}_2\text{Mn}_4 + \alpha\text{-Al} + L$, and at temperature 582.6 °C, mass fraction reaches $f_{\alpha} = 35.32\%$ and $f_{\text{Al}_{15}\text{Si}_2\text{Mn}_4} = 2.68\%$. The third phase, Mg_2Si , starts to form at 582.6 °C according to the reaction $L \rightarrow \text{Al}_{15}\text{Si}_2\text{Mn}_4 + \alpha\text{-Al} + \text{Mg}_2\text{Si} + L$, and solidification finishes at 558.3 °C.

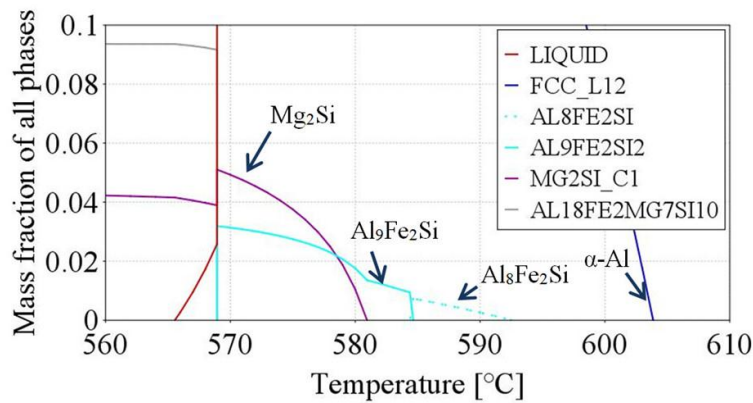


Figure 12. Property diagram for AlMg5Si5Fe1.0 alloy.

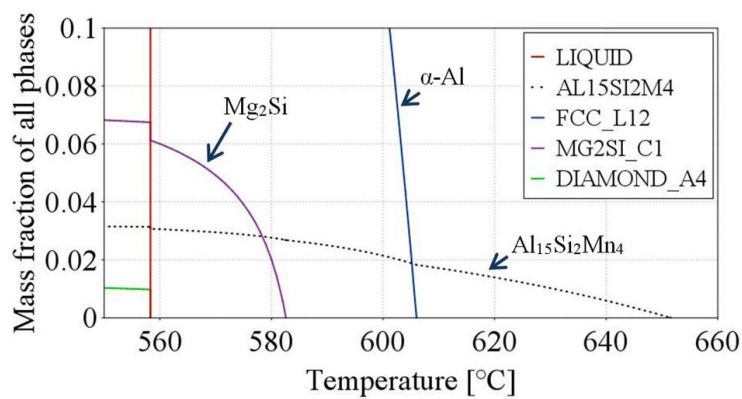


Figure 13. Property diagram for AlMg5Si5Mn1.0 alloy.

The AlMg5Si5Fe1.0Mn1.0 alloy starts to solidify (Figure 14) with the $Al_{15}Si_2Mn_4$ phase at 667.1 °C according to $L \rightarrow Al_{15}Si_2Mn_4 + L$, continuing until 604.2 °C where mass fraction reaches $f_{Al_{15}Si_2Mn_4} = 3.59\%$. The second phase, α -Al, starts to form at 604.2 °C according to $L \rightarrow Al_{15}Si_2Mn_4 + \alpha\text{-Al} + L$, and at the temperature 582.4 °C mass fraction reaches $f_{\alpha} = 33.16\%$ and $f_{Al_{15}Si_2Mn_4} = 5.12\%$. At 582.4 °C, the third phase, magnesium-rich Mg_2Si , begins to form according to the reaction $L \rightarrow Al_{15}Si_2Mn_4 + \alpha\text{-Al} + Mg_2Si + L$, and at the temperature 566.8 °C mass fraction reaches $f_{\alpha} = 74.47\%$, $f_{Al_{15}Si_2Mn_4} = 6.19\%$ and $f_{Mg_2Si} = 5.60\%$. At 566.8 °C, the $Al_{18}Fe_2Mg_7Si_{10}$ intermetallic phase starts to form according to the reaction $L \rightarrow Al_{15}Si_2Mn_4 + \alpha\text{-Al} + Mg_2Si + Al_{18}Fe_2Mg_7Si_{10} + L$ and solidification finishes at 560.7 °C.

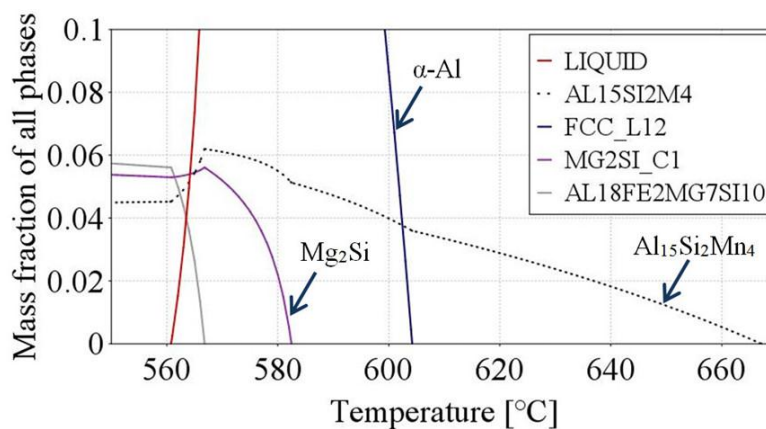


Figure 14. Property diagram for AlMg5Si5Fe1.0Mn1.0 alloy.

4. Discussion

The modification of the microstructure caused by melt stirring requires discussion, especially the transformation from a dendritic structure to rosettes with minor dendrites and, occasionally, spheroids. Here, the measured parameters (dendrite arm spacing, specific surface, length and number density of intermetallics and eutectic spacing) will be analyzed in comparison to literature data, and the various effects of stirring on the studied alloys and growing phases will be discussed.

The non-dendritic morphologies are mostly explained by dendrite fragmentation in presence of forced convection [1]. Mentioned by Flemings [1], the mechanism responsible for fragmentation may be: (a) dendrite arm fracture; (b) remelting of the dendrite root; and/or (c) recrystallization caused by fluid flow inducing mechanical stress.

4.1. Rosettes

The rosette morphology and its growth were studied by Mullis [9] using the cellular automaton method. Mullis observed that forced convection induces rotation of the dendrite tip caused by thermal and solutal advection. The size of the crystal was defined by the magnitude of the bending parameter, and eventually such a rosette might form without external mechanical interaction coming from flow. Birol [10] conducted experiments with metal alloys flowing along a cooled plate, and proved that during flow, crystals have the possibility to collide with each other and coalesce to grow as agglomerates. Therefore, in the final microstructure may be observed fully shaped dendrites, α -Al crystals formed as rosettes, and some globular grains. Niroumand and Xia [11], on microstructure of AlCu10 solidified by stirring, observed many round crystals shaped as clusters. With the help of classical LOM and in 3D, they found out that globular crystals of clusters are connected to each other in three dimensions, even though on a 2D micrograph they can look separate. This means that dendrite fragmentation and subsequent agglomeration influences microstructure formation only weakly, and suggests that rosette-shaped clusters are ripened arms of deformed dendritic crystals.

4.2. Spheroids

Ji et al. [12] theoretically analyzed the stability of the solid–liquid interface during solidification under forced convection. The numerical analysis indicated that the growth morphology may change from equiaxed dendrite to spheroid via rosette when shear rate and turbulence increases significantly. Das et al. [13], using Monte Carlo simulations, showed that a tendency for dendritic growth was reduced and globularization of the primary phase in the melt is caused by the rotation of the solid particle and elimination of constitutional undercooling through reduction of the thermal/solutal diffusion layers at the solid–liquid interface.

In the experiments on rheomoulding, Ji et al. [12] produced a spherical morphology, instead of a rosette or dendrite, by high shear rates. Birol [14] obtained globular structures with forced convection and internal cooling, and proposed that stirring caused the uniform chemical composition near the solid–liquid interface. The results of Li et al. [15] on succinonitrile (SCN)-5% water also supports the hypothesis that nondendritic microstructure comes from natural nucleation and globular growth. Martinez and Flemings' [16] study on AlCu4.5 alloy found that intensive convection may lead to growth in spheroidal form just below the liquidus temperature.

In the current experiment, rosettes seem to form as an effect of rotation of the dendrite tip during growth, and are also ripened arms of deformed dendritic crystals. This explanation is especially supported by the fact that many dendrites were found in addition to overwhelming rosettes. The spheroids seem to be part of the dendrites, because the formation of spheroids requires intensive stirring, causing a very high shear rate.

4.3. Dendrites

In columnar solidification, the microstructure is described with primary dendrite arm spacing λ_1 [17–19] and by secondary dendrite arm spacing λ_2 . For equiaxed grain morphologies resulting from free growth (equiaxed solidification), metallurgists traditionally measure λ_2 and grain size, or number of grains or distance between grains [17]. Recently, the additional measure of specific surface S_v of dendrites was proposed and applied by Voorhees et al. [20].

Secondary dendrite arms start to grow very close to the dendrite tip, initially as perturbations, which develop into cell-like structures and further grow as separate arms located parallel to each other with similar sizes varying with time. The growth by natural thermal convection and solutal fluctuations leads to arms of various sizes, where smaller arms dissolve and the larger overgrow smaller. The distance between secondary arms λ_2 is determined by the coarsening process [21,22]. Many mathematical models [19,23,24] were developed based on the concept that dendrite coarsening is diffusion controlled, but mostly they calculate λ_2 with a simple power law as a function of local solidification time t :

$$\lambda_2 = c_1 \cdot t^{n_1} \quad (1)$$

where $n_1 = 0.33$ for diffusive mass transport and 0.48 for convective regime [25]. c_1 is a coefficient containing material constants (diffusion coefficient, concentration, etc.) and is given different forms by Kattamis and Flemings [23], Voorhees and Glicksman [26], and by Mortensen [27]. Bouchard and Kirkaldy [19,28] proposed a formula based on local cooling rate:

$$\lambda_2 = c_2 \cdot R^{-n_2} \quad (2)$$

where $c_2 =$ coefficient and $n_2 = 0.33$ [19] or is in the range 0.22–0.33 for AlSi alloys [28] with various Si content.

Mullis [29] found that flow from the tip of the secondary arm towards the root will enhance the ripening rate, while flow in the opposite direction will reduce the ripening rate. For flow aligned along primary trunk, all secondary arms will experience a transverse flow, which will enhance ripening. Because of the four-fold symmetry of dendrites, the flow effect on secondary spacing λ_2 could be small (increase in ripening rate).

Diepers et al. [30] developed a model for Ostwald ripening, which holds that in the dependence of secondary spacing λ_2 on solidification time, the exponent n_1 changes from 0.33 for diffusive ripening to 0.5 for flow-governed dendrite ripening because of the flow increase caused by coarsening. The simulation results are in agreement with considerations of Ratke and Thieringer [31] on convective ripening theory and experimental results of Steinbach and Ratke [25] on directional solidification of A357 alloy (AlSi7Mg0.6). Steinbach and Ratke [25] found that λ_2 increases continually with increasing magnetic induction (increasing flow velocities) (e.g., by $t = 1250$ s from 80 μm to 140 μm). According to power law expressions of solidification time and by the c_1 coefficient from [25], here the change in n_1 exponent is from 0.36 in a solute-controlled system with natural convection to 0.48 by flow caused by electromagnetic stirring (6 mT).

In the current equiaxed solidification experiments, with increasing flow, secondary spacing λ_2 decreased from 87 to 77 μm (–12%) for AlSi5Fe1.0 alloy, but remained almost unchanged for the other alloys, which contained Mg and therefore Mg_2Si phases.

Stirring decreased solidification time (Table 1), and according to the Equation (1) for λ_2 , this should mean a decrease in secondary spacing λ_2 . Lower secondary spacing was measured for only AlSi5Fe1.0 alloy, while for other alloys it remained almost unchanged. For the AlSiFe1.0 alloy solidified without stirring, $\lambda_2 = 87$ μm , but with flow, based on measured solidification time, calculated secondary spacing ($\lambda_2 = 82$ μm) is still bigger than measured spacing ($\lambda_2 = 77$ μm). In order to reach the measured value of 77 μm , the exponent n_1 in Equation (1) should be lower, even lower than n_1 for diffusive ripening (without stirring) [25]. These results would require a decrease from 0.33 to 0.318; this is opposed to literature [25,30], suggesting an increase in n_1 caused by convective ripening. For other alloys

(containing Mg), according to Equation (1), shorter solidification time results in a smaller secondary spacing λ_2 , but only slightly smaller. In order to reach, by calculation, the measured λ_2 values, the exponent by stirring should be slightly higher, increasing from 0.33 for diffusive mass transport to the range 0.334–0.342 for convective ripening, and that is much less than the range 0.47–0.50 found in literature [25,30] for directional solidification. This behavior of exponents suggests a lack of forced convection by electromagnetic stirring for Mg-containing alloys, or its significant reduction during coarsening of secondary arms. Instead of $n_2 = 0.33$ in Equation (2), the exponent would be 0.342 for AlSi5Fe1.0 alloy and 0.326–0.318 for Mg-containing alloys. This is in contrast to [25,30], where secondary spacing λ_2 increased considerably under flow during directional solidification

Much of research devoted to dendritic structure was focused on measuring secondary dendrite arm spacing λ_2 , but this measure does not provide information on the complexity of the dendritic structure. Marsh and Glicksman [32] found out that, despite drastic morphological changes from dendritic structure to spheroidal during the coarsening processes, the solidification time t dependence of specific interfacial area S_v was always described as:

$$S_v \sim t^{1/3} \quad (3)$$

Kasperovich and Genau [33] studied mushy zone coarsening for AlCu30 alloy, and S_v was found to be in the range 0.04–0.22 μm^{-1} for holding times from 20 to 500 min. S_v [33] decreased from 0.077 to 0.035 μm^{-1} (for holding time of 200 min) with increasing forced convection generated by 6 mT RMF.

For all alloys studied here, S_v decreased under fluid flow, meaning that the dendrites or rosettes are rounder with stirring. Based on Equation (3) and the solidification time measured, the calculated decrease in S_v is smaller than measured. For AlSi5Fe1.0 alloy with stirring, the measured S_v is 0.019 μm^{-1} , while the calculated value is 0.022 μm^{-1} , and similarly for AlMg5Si5, measured S_v is 0.024 μm^{-1} and calculated S_v is 0.0341 μm^{-1} . The difference between measured (without stirring) and calculated (with stirring) values of S_v seems to present well the effect of stirring on microstructure.

4.4. Eutectics

Eutectic morphologies [17,18] are characterized by the simultaneous growth of two (or more) phases from liquid, where the exchange of solute between two simultaneous phases occurs via transport in the liquid phase, and transport may be strongly influenced by forced convection. The eutectic spacing λ_E was determined by Jackson and Hunt [18,34]:

$$\lambda_E = c_3 \cdot V^{-0.5} \quad (4)$$

where c_3 = coefficient and V solidification front velocity.

Steinbach and Ratke, in directional solidification of A357 alloy, found that fluid flow increased eutectic spacing (e.g., for solidification velocity 90 $\mu\text{m}/\text{s}$, spacing increased from 3 to 7 μm), and also reported the reduction in λ_E with increasing solidification velocity according to the well-known Jackson and Hunt relation (4). In directional solidification of AlSi5/7/9Fe0.2/0.5/1.0 alloys [35], the eutectic spacing did not show any clear correlation with fluid flow, which was in agreement with earlier results by Sous [36].

As an example, eutectic solidification for AlSi5Fe1.0 [8] occurs at the final eutectic reaction at 575 °C. During directional solidification with a temperature gradient of 3 K/mm, the mushy zone is about 18 mm wide [8], while the eutectic zone is about 1–3 mm wide and the flow deep between dendrites might be reduced. However, in the current equiaxed solidification with a temperature gradient of 0.143–0.214 K/mm and cooling rate of 0.112–0.626 K/s, equiaxed dendrites grew freely in the mush, moving in the liquid with similarly growing eutectic phases, so one cannot expect that convection is diminished by dendrites. From Table 1, it is clear that for AlSi5Fe1.0, forced convection increases the eutectic spacing λ_E by about 9%. For the other alloys, the change in spacing is similar in magnitude, but both increases and decreases were observed. For alloys with either Fe or Mg, we saw

an increase, while for alloys containing both Fe and Mg, flow reduces the spacing. It seems that some common influence of both elements causes such an effect on growing phases. The unclear effect of stirring on the eutectic spacing may come from the small amount of eutectic and the resulting small number of measurements. The mass fraction for eutectic reached 4.67 wt. % in AlSi5Fe1.0 and only about 1.5–2.1 wt. % in Mg-containing alloys, whilst Mg₂Si reached about 7.8 wt. % [7].

The Mg₂Si phases also seem to be affected by convection that causes about a 5%–10% increase in spacing $\lambda_{\text{Mg}_2\text{Si}}$. There are no literature data concerning fluid flow effects on Mg₂Si phases.

4.5. Intermetallics

The shortening of β phases observed in this work is consistent with results by Nafisi et al. [37], where, for specimens solidified in a sand mold, stirring decreased average length from $L_\beta = 9\text{--}10\ \mu\text{m}$ to $7\text{--}8\ \mu\text{m}$, and respectively in a copper mold decreased weakly in the range $L_\beta = 4.5\text{--}5\ \mu\text{m}$. Fang et al. [38], for LM25 alloy (AlSi7Mg0.2–0.6Fe0.5), found a shortening of β phases (from 75 to 15 μm), and for LM24 alloy (AlSi8Cu3Fe1.3), β -Al₅FeSi with lengths 95–110 μm were completely eliminated. Steinbach et al. [39] observed that flow causes the formation of a eutectic center region in directionally solidified AlSi7Fe1.0 alloy and growth of about 280 μm long Fe platelets, while the same system without stirring precipitated shorter β phases of about 160 μm long. In [40], forced convection in directional solidification of AlSi5/7/9Fe0.2/0.5/1.0 alloys caused about 20% shortening of β phases in the dendritic region of the specimen and 9% increase in the eutectic reach center. The histograms displayed that the most common are β phases with lengths from 5 to 40 μm , and that convection led to a higher number of short phases, causing a smaller average length L_β .

Nafisi et al. [37], for AlSi6.8Fe0.8 alloy, showed an increase under stirring in the number density for sand mold from $n_\beta = 600\text{--}1200\ \text{mm}^{-2}$ to $n_\beta = 800\text{--}2600\ \text{mm}^{-2}$, and copper mold from $n_\beta = 5000\text{--}13,000\ \text{mm}^{-2}$ to $n_\beta = 5000\text{--}14,000\ \text{mm}^{-2}$. The data in [40] clearly showed an increase in number density n_β , stronger in the eutectic center (42%) than in the outer part (17%) of the specimens.

The analysis of the stirring effect in directional solidification of AlSiFe alloys [40] has pointed to shortening of β phases as a complicated effect of forced convection, solute segregation, dendrites, and intermetallic morphology. Fragmentation and partial dissolution of β -Al₅FeSi acting as nucleation sites were explained as a cause of higher number density n_β and a decrease in β platelet length L_β .

4.6. Solidification by Stirring

For AlSi5Fe1.0 alloy (Table 1), stirring decreased secondary spacing λ_2 from 87 to 77 μm (–12%), changed S_v from 0.023 to 0.019 μm^{-1} , shortened β phases from 71 to 57 μm (–20%), increased its number density from 109 to 160 mm^{-2} , and increased eutectic spacing from 8.5 to 9.5 μm . According to the property diagram (Figure 9), α -Al started to form first at 627.4 °C, next was β -Al₅FeSi at 608.4 °C, and, finally, eutectics precipitated at 575 °C. Flow determined growth of α -Al, causing rosettes formation, minor dendrites, and, occasionally, spheroids, and changed secondary spacing λ_2 . β phases started to grow when the solid mass fraction of α -Al reached 40%, which means the shortening of β occurred between well-formed dendrites (at least precipitated in 40%). The occurrence of such a large amount of α -Al phase probably decelerated flow and might support mechanical interactions between α -Al dendrites and moving β . Eutectics precipitated at the end and the flow was probably strongly reduced by dendrites and β , so the increase in eutectic spacing λ_E was influenced by local small flows between solid phases.

For AlMg5Si5 alloy (Table 1), stirring produced a negligible change in measured λ_2 from 67 to 68 μm , decreased S_v from 0.036 to 0.024 μm^{-1} , and decreased eutectic spacing from 9.8 to 8.8 μm . According to Figures 10 and 11, α -Al started to form first at 608.0 °C, next was the Mg₂Si phase at 581.7 °C, and, finally, eutectics precipitated at 558.6 °C. The growth of α -Al seems to be undisturbed by Mg₂Si until 581.7 °C, and until the fraction of α -Al $f_\alpha = 37.28\%$, mostly rosettes were formed. The arm-ripening was influenced by fluid flow for AlSi5Fe1.0 alloy, but for AlMg5Si5 stirring was probably diminished by Mg₂Si phases, and convection changed secondary dendrite arm spacing λ_2 only slightly.

For AlMg5Si5Fe1.0 alloy (Table 1), forced convection modified λ_2 only from 60 to 62 μm , S_v from 0.034 to 0.026 μm^{-1} , decreased eutectic spacing from 11.7 to 6.8 μm , and changed Mg_2Si spacing from 11.7 to 12.7 μm . According to the property diagram (Figure 12), α -Al started to form first at 603.8 °C, next was β - Al_5FeSi phase at 592.5 °C, next was Mg_2Si at 580.9 °C, and, finally, eutectics precipitated at 565.5 °C. The growth of α -Al seems to be undisturbed by β - Al_5FeSi until 592.5 °C and by Mg_2Si until 580.8 °C, and rosettes formed but λ_2 changed only weakly. A 5% shortening of the β - Al_5FeSi phase and increase in number density n_β (14%) seems to be affected by growing Mg_2Si , in comparison to AlSi5Fe1.0 alloy. Initially, β grew between α -Al, but further in the presence of Mg_2Si , which seems to have decreased forced convection and reduced the possible modification of β - Al_5FeSi . The flows in almost-solidified alloys are probably very small, but still have potential to influence the Mg_2Si and eutectic spacing.

For AlMg5Si5Mn1.0 alloy (Table 1), when stirring is applied, there is no change in measured λ_2 , a decrease in S_v from 0.036 to 0.028 μm^{-1} , an increase in eutectic spacing from 7.5 to 8.7 μm , and an increase in Mg_2Si spacing from 11.6 to 12.0 μm . For Mn-rich phases, flow decreased the average overall dimension by about 9% from 299 to 273 μm and increased number density n_{Mn} from 20 to 27 mm^{-2} . According to the property diagram (Figure 13), the first thing to form was the Mn-rich phase $\text{Al}_{15}\text{Si}_2\text{Mn}_4$ at 651.6 °C, next was α -Al at 606.0 °C, third was Mg_2Si at 582.6 °C, and, finally, eutectics precipitated at 558.3 °C. About 60% (Figure 13) of Mn-rich phases grew freely in liquid melt and, under forced convection, formed as smaller structures. Similar to previous Mg-containing alloys, calculated λ_2 changed only weakly under reduced forced convection. Growth of initial Mn-rich phases influenced flow very slightly and allowed for rosette formation. Mn-rich phases precipitated gradually during solidification in liquid melt as complicated structures, being overgrown by dendrites (Figure 8a) and later grew between dendrites and Mg_2Si (Figure 8b).

For AlMg5Si5Fe1.0Mn1.0 alloy (Table 1), stirring produced no change in measured λ_2 , a decrease in S_v from 0.035 to 0.028 μm^{-1} , an increase in eutectic spacing from 8.1 to 9.1 μm , and in Mg_2Si spacing from 11.3 to 12.1 μm . Forced convection produced the growth of α -Al rosettes, β phases with unmodified length L_β , but with increased number density n_β . Mn-rich phases growing early during solidification, before or with α -Al, have not influenced melt flow, or the influence is small. Convection was therefore not disturbed in the early stage of solidification, causing formation of rosettes. Flow disturbed by Mg_2Si during the late stage of solidifications influenced the ripening process slightly and resulted in only a small difference between the secondary spacing λ_2 calculated from (1) and the measured value. Mg_2Si phases, reducing flow, clearly limited shortening of β - Al_5FeSi phases, but did not stop the increase in number density n_β .

Flow decreased secondary dendrite arm spacing λ_2 in AlSi5Fe1.0 alloy (without Mg) and only very slightly in Mg-containing alloys. Mg_2Si diminished flow and convective ripening while supporting diffusive mass transport. α -Al grew as rosettes with modified S_v in all studied alloys. The decrease in S_v became weaker with growing complexity of alloy (growing number of elements), and for AlMg5Si5, S_v decreased by 33%, whilst decreasing by 20% for AlMg5Si5Fe1.0Mn1.0 alloy.

The current study confirmed the results [40] for directional solidification of AlSi5Fe1.0 alloy, where forced convection decreased average length L_β of β phases by about 20% and increased number density n_β by about 17% under comparable rotational speed of 2 s^{-1} . Completely new is that the flow effect was observed in equiaxed growth by low temperature gradient and low cooling rate, where there is no possibility of phases remelting. This suggests shortening of β as an effect of mechanical fragmentation or mechanism determined by solute distribution changed under flow.

For AlSi5Fe1.0 alloy, flow caused a 20% decrease of average length L_β of β phases and 47% increase in number density n_β , whilst for AlMg5Si5Fe1.0, L_β decreased only 5% and n_β increased 14%. Flow effect on β is weaker in Mg-containing alloys, as a result of reducing the flow by Mg_2Si . For AlMg5Si5Fe1.0Mn1.0, L_β decreased only 2% and n_β increased 77%. By measured length L_β , number density n_β , and non-inspected thickness of β , a larger number of shorter phases by the same

Fe quantity were included in β -Al₅FeSi, which means that β must be thinner. This mechanism is unclear and needs more experimental and analytical investigations.

5. Conclusions

1. Electromagnetic stirring caused a transformation in microstructure from equiaxed dendritic to rosettes with minor dendrites as an effect of rotation of dendrite tips and ripening arms of deformed dendrites. Occasionally occurring spheroids seem to be part of deformed dendritic crystals.

2. Stirring caused a decrease in solidification time for all alloys. Contrary to what has previously been reported in the literature, flow decreased secondary dendrite arm spacing λ_2 for AlSi5Fe1.0 alloy. Even considering the lower solidification time, the exponents in the power law equation for λ_2 changed values: n_1 from 0.33 to 0.318 and n_2 from 0.33 to 0.342. For Mg-containing alloys, measured secondary spacing λ_2 was almost unchanged, but considering lower solidification time and lower calculated λ_2 , the exponents should change: n_1 from 0.33 to 0.334–0.342, and n_2 from 0.33 to 0.326–0.318, less than in previous works.

3. Specific surface S_v decreased under forced flow and clearly signaled the modification of microstructure caused by stirring.

4. Forced convection decreased the length of β -Al₅FeSi (20%) and increased number density (47%) in AlSi5Fe1.0 alloy in equiaxed solidification, in accordance with literature data for directional solidification. In Mg-containing alloys, the changes were much smaller.

5. Stirring decreased length of Mn-rich phases (9%) and increased number density (35%) in AlMg5Si5Mn1.0 alloy.

6. Melt flow changed eutectic spacing λ_E depending on alloy composition, while λ_{Mg_2Si} increased weakly for all alloys.

7. Mg₂Si phases reduced fluid flow generated by RMF and consequentially reduced shortening of β -Al₅FeSi phases, diminished secondary arm ripening caused by forced convection, and supported diffusive ripening. Mg₂Si did not disturb transformation from dendrites to rosettes under flow.

8. Shortening of β -Al₅FeSi phases caused by stirring occurred in equiaxed solidification without remelting, probably by mechanical fragmentation, modified solute distribution, and additional nucleation sites.

9. Stirring application and efficiency in microstructure modification depends on chemical composition, precipitating phases (e.g., Mg₂Si), and growth sequence of phases in alloys.

Acknowledgments: The research leading to these results has received funding from the People Programme (Marie Curie Actions) of the European Union's Seventh Framework Programme (FP7/2007-2013) under REA grant agreement No. PCIG13-GA-2013-613906. Thanks are due to Mark Morton from Hydro Aluminum High Purity GmbH (Grevenbroich, DE) for the aluminum.

Conflicts of Interest: Funding sponsor is European Union's Seventh Framework Programme (FP7/2007-2013). The funding sponsors had no role in the design of the study; in the collection, analysis, or interpretation of data; in the writing of the manuscript, and in the decision to publish the results.

References

1. Flemings, M. Behavior of metal alloys in the semisolid state. *Metall. Mater. Trans. B* **1991**, *22*, 269–293. [[CrossRef](#)]
2. Kiuchi, M.; Kopp, R. Mushy/semi-solid metal forming technology—present and future. *CIRP Ann. Manuf. Technol.* **2002**, *51*, 653–670. [[CrossRef](#)]
3. Gawroński, J.; Szajnar, J. Properties of Mo59 brass solidification in magnetic field. *Solidif. Met. Alloy.* **1998**, *37*, 131–138.
4. Szajnar, J. The columnar crystals shape and castings structure cast in magnetic field. *J. Mater. Process. Technol.* **2004**, *157–158*, 761–764. [[CrossRef](#)]
5. Shabestari, S.G. The effect of iron and manganese on the formation of intermetallic compounds in aluminum-silicon alloys. *Mater. Sci. Eng. A* **2004**, *383*, 289–298. [[CrossRef](#)]

6. Gustafsson, G.; Thorvaldsson, T.; Dunlop, G.L. The influence of Fe and Cr on the microstructure of cast Al-Si-Mg alloys. *Metall. Mater. Trans. A* **1986**, *17*, 45–52. [[CrossRef](#)]
7. Thermo-Calc 4.1–Software Package from Thermo-Calc Software AB. Stockholm, Sweden. Available online: <http://www.thermocalc.se> (accessed on 12 March 2015).
8. Mikolajczak, P.; Ratke, L. Thermodynamic assessment of mushy zone in directional solidification. *Arch. Foundry Eng.* **2015**, *15*, 101–109. [[CrossRef](#)]
9. Mullis, A. Growth induced dendritic bending and rosette formation during solidification in a shearing flow. *Acta Mater.* **1999**, *47*, 1783–1789. [[CrossRef](#)]
10. Birol, Y. A357 thixoforming feedstock produced by cooling slope casting. *J. Mater. Process. Technol.* **2007**, *186*, 94–101. [[CrossRef](#)]
11. Niroumand, B.; Xia, K. 3D study of the structure of primary crystals in a rheocast Al-Cu alloy. *Mater. Sci. Eng. A* **2000**, *283*, 70–75. [[CrossRef](#)]
12. Ji, S.; Fan, Z.; Bevis, M.J. Semi-solid processing of engineering alloys by a twin-screw rheomoulding process. *Mater. Sci. Eng. A* **2001**, *299*, 210–217. [[CrossRef](#)]
13. Das, A.; Ji, S.; Fan, Z. Morphological development of solidification structures under forced fluid flow: A Monte Carlo simulation. *Acta Mater.* **2002**, *50*, 4571–4585. [[CrossRef](#)]
14. Birol, Y. Evolution of globular microstructures during processing of aluminum slurries. *Trans. Nonferrous Met. Soc. China* **2013**, *23*, 1–6. [[CrossRef](#)]
15. Li, T.; Lin, X.; Huang, W. Morphological evolution during solidification under stirring. *Acta Mater.* **2006**, *54*, 4815–4824. [[CrossRef](#)]
16. Martinez, R.A.; Flemings, M.C. Evolution of particle morphology in semisolid processing. *Metall. Mater. Trans. A* **2005**, *36*, 2205–2210. [[CrossRef](#)]
17. Kurz, W.; Fisher, D. *Fundamentals of Solidification*; Trans Tech Public.: Zurich, Switzerland, 1992; pp. 85–90.
18. Dantzig, J.A.; Rappaz, M. *Solidification*; EPFL Press: Lausanne, Switzerland, 2009.
19. Stefanescu, D. *Science and Engineering of Casting and Solidification*; Springer Science+Media Business: New York, NY, USA, 2009. [[CrossRef](#)]
20. Mendoza, R.; Alkemper, J.; Voorhees, P. The morphological evolution of dendritic microstructures during coarsening. *Metall. Mater. Trans. A* **2003**, *34*, 481–489. [[CrossRef](#)]
21. Hunt, J.D. Pattern formation in solidification. *Sci. Technol. Adv. Mater.* **2001**, *2*, 147–155. [[CrossRef](#)]
22. Hunt, J.D.; Lu, S.Z. Numerical modeling of cellular/dendritic array growth: Spacing and structure predictions. *Metall. Mater. Trans. A* **1996**, *27*, 611–623. [[CrossRef](#)]
23. Kattamis, T.Z.; Flemings, M.C. Dendrite morphology, Microsegregation and Homogenization of low alloy steel. *Trans. Met. Soc. AIME* **1965**, *233*, 992–999.
24. Rappaz, M.; Boettinger, W. On dendritic solidification of multicomponent alloys with unequal liquid diffusion coefficients. *Acta Mater.* **1999**, *47*, 3205–3219. [[CrossRef](#)]
25. Steinbach, S.; Ratke, L. The influence of fluid flow on the microstructure of directionally solidified AlSi-base alloys. *Metall. Mater. Trans. A* **2007**, *38*, 1388–1394. [[CrossRef](#)]
26. Voorhees, P.W.; Glicksman, M.E. Ostwald ripening during liquid phase sintering—Effect of volume fraction on coarsening kinetics. *Metall. Mater. Trans. A* **1984**, *15*, 1081–1089. [[CrossRef](#)]
27. Mortensen, A. On the rate of dendrite arm coarsening. *Metall. Mater. Trans. A* **1991**, *22*, 569–574. [[CrossRef](#)]
28. Bouchard, D.; Kirkaldy, J.S. Prediction of dendrite arm spacing in unsteady- and steady-state heat flow. *Metall. Mater. Trans. B* **1997**, *28*, 651–663. [[CrossRef](#)]
29. Mullis, A.M. The effects of fluid flow on the secondary arm coarsening during dendritic solidification. *J. Mater. Sci.* **2003**, *38*, 2517–2523. [[CrossRef](#)]
30. Diepers, H.J.; Beckerman, C.; Steinbach, I. Simulation of convection and ripening in a binary alloy mush using the phase field method. *Acta Mater.* **1999**, *47*, 3663–3678. [[CrossRef](#)]
31. Ratke, L.; Thieringer, W.K. The influence of particle motion on Ostwald ripening in liquids. *Acta Mater.* **1985**, *33*, 1793–1802. [[CrossRef](#)]
32. Marsh, S.P.; Glicksman, M.E. Overview of geometric effects on coarsening of mushy zones. *Metall. Mater. Trans. A* **1996**, *27*, 557–567. [[CrossRef](#)]
33. Kasperovich, G.; Genau, A.; Ratke, L. Mushy zone coarsening in an AlCu₃₀ alloy accelerated by a rotating magnetic field. *Metall. Mater. Trans. A* **2011**, *42*, 1657–1666. [[CrossRef](#)]
34. Jackson, K.A.; Hunt, J.D. Lamellar and rod eutectic growth. *Trans. AIME* **1966**, *236*, 1129–1142.

35. Mikolajczak, P.; Ratke, L. Intermetallic phases and microstructure in AlSi alloys influenced by fluid flow. In *The Minerals, Metals & Society TMS*; John Wiley & Sons. Inc.: San Francisco, CA, USA, 2011. [[CrossRef](#)]
36. Sous, S. Instationäre Erstarrung Eutektischer Al-Si Legierungen. Ph.D. Thesis, RWTH, Aachen, Germany, 2000.
37. Nafisi, S.; Emad, D.; Shehata, T.; Ghomashchi, R. Effects of electromagnetic stirring and superheat on the microstructural characteristics of Al-Si-Fe alloy. *Mater. Sci. Eng. A* **2006**, *A432*, 71–83. [[CrossRef](#)]
38. Fang, X.; Shao, G.; Liu, Y.Q.; Fan, Z. Effects of intensive forced melt convection on the mechanical properties of Fe containing Al-Si based alloys. *Mater. Sci. Eng. A* **2007**, *445–446*, 65–72. [[CrossRef](#)]
39. Steinbach, E.N.; Witusiewicz, V.; Sturz, L.; Ratke, L. Fluid flow effects on intermetallic phases in Al-cast alloys. *Trans. Indian Inst. Met.* **2007**, *60*, 137–141. [[CrossRef](#)]
40. Mikolajczak, P.; Ratke, L. Effect of stirring induced by rotating magnetic field on β -Al₅FeSi intermetallic phases during directional solidification in AlSi alloys. *Int. J. Cast Met. Res.* **2013**, *26*, 339–353. [[CrossRef](#)]



© 2017 by the author. Licensee MDPI, Basel, Switzerland. This article is an open access article distributed under the terms and conditions of the Creative Commons Attribution (CC BY) license (<http://creativecommons.org/licenses/by/4.0/>).